International Journal of Mass Spectrometry 303 (2011) 164–172

Contents lists available at ScienceDirect

International Journal of Mass Spectrometry

journal homepage: www.elsevier.com/locate/ijms

Thermal desorption metastable atom bombardment ionization aerosol mass spectrometer

Carly B. Robinson[a,b], Joel R. Kimmel[b,c,d,*], Donald E. David[a,b], John T. Jayne[c], Achim Trimborn[c], Douglas R. Worsnop[c], Jose L. Jimenez[a,b]

[a] Department of Chemistry and Biochemistry, University of Colorado, Boulder, CO, United States
[b] Cooperative Institute for Research in Environmental Sciences (CIRES), University of Colorado, Boulder, CO, United States
[c] Aerodyne Research Inc., Billerica, MA, United States
[d] Tofwerk AG, Thun, Switzerland

ARTICLE INFO

Article history:
Received 13 December 2010
Received in revised form 25 January 2011
Accepted 29 January 2011
Available online 15 February 2011

Keywords:
Metastable atom beam source
Metastable atom bombardment (MAB) ionization
Aerosol mass spectrometry

ABSTRACT

A metastable atom bombardment (MAB) ionization source has been coupled to an existing thermal desorption aerosol mass spectrometer. The design allows real-time alternation between MAB and electron ionization (EI). A jet of metastable species produced in a DC discharge is directed at the ionization volume of the mass spectrometer, where Penning ionization is thought to be the dominant mechanism. Performance is characterized in experiments with oleic acid particles. By changing discharge gases between N_2, Kr, and Ar, the excited state energy of the metastable species can be adjusted in the range 8.5–11.7 eV. For vaporization at 180 °C, all gases yield significantly less fragmentation than EI, which could improve results of factor analysis. Fragmentation increases with vaporization temperature, but generated fragments have higher average mass than those produced by EI. Analyte signal levels are 0.1% and 0.006% of equivalent analysis with EI when using Ar^* and Kr^*, respectively. These sensitivities are not practical for ambient studies, but are sufficient for source measurements, as demonstrated with direct measurements of biomass burning emissions. The measured Ar^* flux of 3.6×10^{13} sr^{-1} s^{-1} is ~30 times lower than the best literature values for similar metastable beam sources, suggesting that sensitivity can be increased by source design improvements.

1. Introduction

Aerosols have important effects on regional and global climate, visibility, and human health. At present aerosols are considered by the Intergovernmental Panel on Climate Change as the most uncertain component in the radiative forcing of climate [1]. Atmospheric aerosols are mixtures of organic and inorganic matter. The inorganic fraction is better understood, due to the smaller number of species, fewer sources, and simpler chemistry. Organic aerosols (OA), on the other hand, are complex mixtures of a wide variety of species with both natural and anthropogenic sources. Thorough chemical characterization of OA remains a significant challenge, and the sources and processing of OA are poorly known. This leads to inaccuracies in predictions of future climate forcing and requires new approaches for the analysis of OA [2].

A number of techniques can quantify and characterize OA, but inevitably each technique has limitations. Thermal–optical instruments can quantify total organic carbon [3], while total water-soluble organic carbon can be quantified via capture into a liquid and online analysis [4]. However both techniques are limited by their lack of chemical resolution, as they cannot identify subtypes of OA. Ideally OA could be characterized at a molecular level, but due to the extreme range of physical and chemical properties of OA species, only a small fraction of the mass of ambient OA has been compositionally resolved [2,5]. Several approaches attempt to characterize the composition of the total bulk OA, although at the expense of molecular information. These include FTIR [6], NMR [7], and online aerosol mass spectrometers, such as the Aerodyne aerosol mass spectrometer (AMS) used in this work [8]. The AMS flash vaporizes particles and ionizes the gaseous plume with electron ionization (EI). Recorded MS signals are quantitatively apportioned to total OA and non-refractory inorganic species. Factor analysis of AMS data allows the identification of several OA components which provide useful information about OA sources and processing [8]. But, the high degree of molecular fragmentation generated by EI limits the information that can be extracted about molecular composition as well as source identification.

Better resolution of different sources of OA and classes of compounds comprising OA is highly desirable. Softer ionization

* Corresponding author at: Aerodyne Research Inc., 45 Manning Road, Billerica, MA 01821-3976, United States.
E-mail address: jkimmel@aerodyne.com (J.R. Kimmel).

1387-3806/$ – see front matter © 2011 Elsevier B.V. All rights reserved.
doi:10.1016/j.ijms.2011.01.027

techniques reduce or eliminate molecular fragmentation by imparting much less energy than EI during the ionization process. Vacuum ultraviolet (VUV) photoionization [9], chemical ionization [10–13], and low energy electron capture ionization [14] have all been recently applied to OA analysis in the laboratory. Even for a softer ionization source the mass spectra of ambient OA are extremely complex. Thus, for a direct analysis instrument like the AMS the main advantage of the more distinct mass spectra would be identification of additional chemical classes of atmospheric OA via factor analysis methods [15]. The AMS represents a well-developed platform for atmospheric aerosol analysis [8], and thus the implementation of a soft-ionization source is simplified. A previous effort coupled a VUV lamp to the thermal desorption AMS platform [16]. The VUV–AMS showed much reduced fragmentation compared to EI, but the sensitivity was 0.02% of EI. Currently a significantly more intense VUV lamp is not available that would allow for increased sensitivity.

This work develops and characterizes hardware for analysis of the AMS-vaporized aerosols by Penning ionization and mass spectrometry. The mechanism of Penning ionization imparts analyte molecules with energies near those imparted by VUV photoionization, and, to a first approximation, one could expect mass spectra generated by the two methods to be qualitatively similar. Penning ionization involves reaction of an analyte molecule (BC) with an excited-state, metastable molecule or atom (A^*) [17,18]. If the ionization potential of the analyte is lower than the internal energy of the metastable species, an electron from the analyte molecule may transfer to a low-lying state of the metastable species forming an analyte cation and causing the loss of the excited electron from the metastable species.

$$A^* + BC \rightarrow A + BC^+ + e^- \quad (1)$$

For cases where the internal energy of the metastable species is significantly greater than the ionization potential of the analyte, the generated cation may fragment:

$$BC^+ \rightarrow B^+ + C \quad (2)$$

Metastable species are commonly formed via controlled gas discharges. For cases where the discharge medium is a pure gas, one can theoretically tailor conditions to yield ionization with minimal fragmentation [19] and/or to ionize only select classes of molecules. In this work we use gases with excited state energies between 8.45 eV (N_2^*) [20,21] and 11.72 eV (Ar^*) [22], which are well suited for the typical ionization energies of organic molecules (9–11 eV) [23].

Current literature includes reports of many new atmospheric pressure ionization schemes that rely on the controlled production of metastable species. In some cases, analyte molecules are ionized directly by Penning ionization [24,25] while other mechanisms involve the Penning ionization of a reagent gas and subsequent ionization of the analyte by chemical ionization mechanisms [26,27]. This work targets the analysis of aerosols vaporized in the ionization volume of the AMS, which must be maintained under high vacuum. In 1993, Faubert et al. [22] demonstrated a new concept for Penning ionization at low pressure, which they termed metastable atom bombardment (MAB) ionization. The design was based on the metastable beam sources of Fahey [28] and Searcy [29], where a low voltage (300–1000 V) corona discharge is maintained between a sharpened needle and a skimmer electrode separated by a sonic nozzle. The sharpened electrode resides in a chamber containing a pure gas at 10–100 mbar and the skimmer electrode resides in an independently pumped stage. Expansion through the nozzle creates a jet containing metastable, neutral, and charged species. The core of the jet passes through the skimmer, and into the low pressure ionization volume of the mass spectrometer. By using electric fields [30] to remove charged species, the MAB ionization source created an ionization environment that was less complex than standard glow discharge methods in which the analyte is introduced into the discharge region. In this first application of the metastable beam source to mass spectrometry, Faubert et al. demonstrated the ability to tune ionization energy and the degree of fragmentation by changing the discharge gas (He, Ne, Ar, and Kr) and they reported sensitivities for organic molecules that were approximately 20% of EI. Little has been published on the use of MAB ionization since that time. Most recently Le Vot et al. have coupled a MAB source to an FTICR mass spectrometer and achieved reported sensitivities comparable to EI [31], and a metastable beam source has recently been used for Ar^* induced fragmentation of peptide ions in a linear ion trap [32].

In this work we have coupled a metastable beam source with an AMS to provide an instrument, termed the MAB–AMS, which measures the mass spectra of aerosol organic species with much reduced molecular fragmentation. The design of the implemented source is presented, key operating parameters are characterized, and the sensitivity and degree of fragmentation of the MAB–AMS are compared with those of the EI–AMS and of a previously published VUV–AMS coupling [16].

2. Experimental methods

The AMS hardware and its application were detailed in a recent review [8], and the time-of-flight AMS is shown in Fig. S1 (supp. Info.). Briefly, ambient particles are sampled directly from atmospheric pressure into the vacuum system of the AMS via an aerodynamic lens [33], which focuses particles into a tight beam. The beam traverses a high vacuum particle flight chamber. A rotating mechanical chopper at the beginning of the particle time-of-flight region can modulate the beam for size-resolved measurements (PToF mode). Alternatively, this chopper is alternated between discrete beam transmitting and non-transmitting positions for background-subtracted ensemble measurements (MS mode). At the end of the particle drift region, particles impact a heated surface (typically 600 °C) which leads to vaporization of non-refractory species. In the standard implementation [8], the resultant plume of vapor is analyzed by electron ionization (EI) mass spectrometry. Typically the filament used to create the electrons for EI has an emission current of 2.0 mA. The AMS (Aerodyne Research, Billerica, MA) is available with three different mass spectrometers: a quadrupole mass spectrometer [34] (QMG 422, Balzers, Furstentum, Liechtenstein), a compact, high-sensitivity TOF mass spectrometer [35] (CTOF, Tofwerk AG, Thun, Switzerland), or a high-resolution TOFMS [36] (HTOF, Tofwerk). This work used the HTOF-based instrument, called the HR-ToF-AMS [36], but the MAB source design is not specific to this platform.

A schematic representation of the metastable beam source and the ionization region of the AMS is shown in Fig. 1. The standard AMS has two EI filaments mounted on opposite sides of the ionization chamber. Here, one filament has been removed, and the metastable beam enters the ionization chamber through a 5 mm diameter hole in the ionization chamber at the position of the removed filament. The self-contained beam source is housed in a stainless-steel vacuum chamber (mechanical drawing available in Fig. S2), which attaches to the AMS vacuum system at an ISO-63 port immediately adjacent to the EI-vaporizer assembly. The beam-exit end of the source chamber extends into the AMS ionization chamber on an axis exactly opposite the remaining EI filament, to the point where the exit aperture of the source is in near contact with the ionization chamber assembly. Metastable species enter the ionization volume a few millimeters from the vaporizer surface. EI is kept inactive during MAB operation. The sensitivity of EI analysis is not significantly affected by the installation of the MAB source.

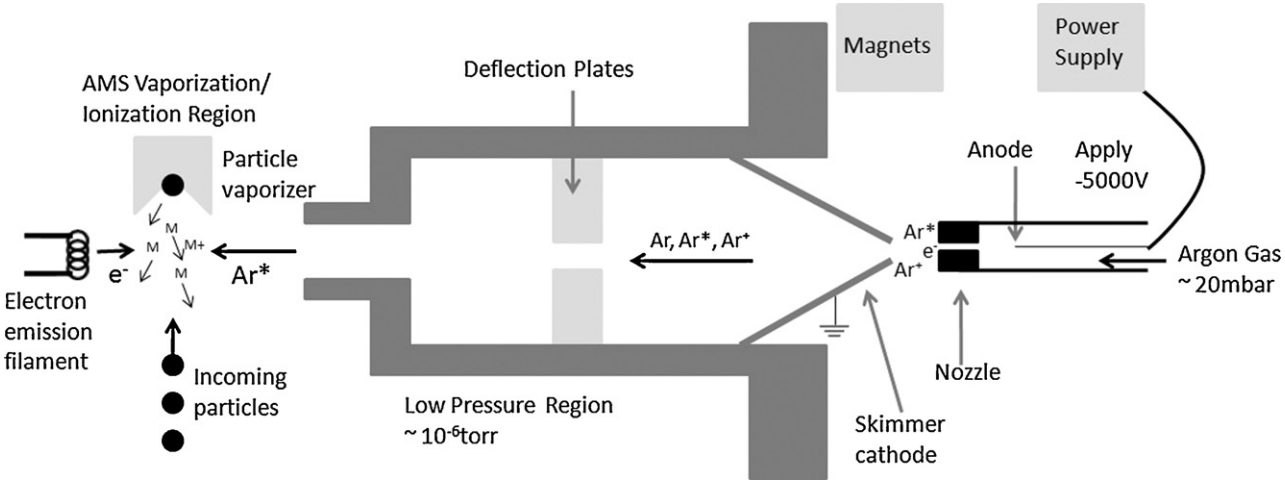

Fig. 1. Schematic of the metastable beam source coupled to the AMS ionization region.

The principles of the metastable beam source were described in Section 1, and the employed design follows the work of Fahey [28], with minor modifications detailed here. The discharge is maintained between a sharp, 1 mm diameter tungsten cathode and a grounded stainless steel skimmer anode. The cathode is housed in a glass tube, referred to as the cathode chamber, having a 330 μm diameter boron nitride nozzle at its exit. The pressure of the cathode chamber (typically 20 mbar) is monitored with a capacitance manometer (MKS Baratron, Andover, MA) and regulated by adjusting the flow of the discharge gas (argon, krypton, and nitrogen, each 99.9997%, research grade, Airgas, Boulder, CO) into the chamber. The glass cathode chamber extends into the stainless steel source chamber through an Ultra-Torr (Swagelok, http://www.swagelok.com) 0.5 inch fitting on the front flange. This flange is moveable in the *X*–*Y* plane and its position can be adjusted during operation to ensure optimum *X* and *Y* alignment of the nozzle and the skimmer aperture [37]. The lateral distances (*Z* axis) between the cathode tip and the nozzle and nozzle and the skimmer are also adjustable, although only when the system is not under vacuum. The region between the nozzle and the skimmer anode is pumped by a 250 L s^{-1} turbomolecular pump (V301, Varian Inc, Lake Forest, CA); pressure is not monitored but is estimated to be near 10^{-3} mbar. To initiate the discharge a voltage of approximately −5000 V is applied to the cathode using a high voltage DC power supply in current-controlled mode (Series FC, Glassman, High Bridge, NJ). After the discharge is struck, the voltage drops to approximately −800 V (depending on conditions) and a constant current is maintained. Discharges generated by this method have been reported to have metastable atom fluxes up to 10^{14} atoms sr^{-1} s^{-1} for argon [28] and 10^{15} atoms sr^{-1} s^{-1} helium [22] and to be stable (<5% variation in current) for durations in excess of one week [38].

The core of the expansion jet created by the nozzle passes through the 1 mm aperture of the stainless steel skimmer anode, and enters the expansion chamber which contains two 16 mm × 16 mm deflection plates separated by 13.5 mm. As indicated in Fig. 1, this expansion chamber extends into the AMS vacuum chamber. The housing of the expansion chamber is perforated, so that its volume is pumped by the AMS vacuum system, and the pressure is assumed to be equal to that of the AMS ionization region (10^{-5}–10^{-6} mbar). A magnet is mounted to the outside of stainless steel beam source chamber, just above the expansion chamber, producing a magnetic field of ~0.02 T at the beam axis. The magnet is used in combination with the deflection plates (typically 100 V difference) to deflect charged species (e.g., Ar^+ and electrons) off the axis of the ionization chamber. Within the ionization chamber, metastable species react with gas-phase molecules from the vaporized aerosols, producing ions which are then analyzed by the mass spectrometer.

The source allows real time alternation between MAB ionization and EI. For long timescale alternation, the discharge and EI filament can simply be turned on and off. For more rapid alternation, both the discharge and the filament remain on. EI operation is toggled on and off by switching the electron acceleration energy between 70 eV (on) and 0 eV (off). For time periods where the electron energy is 0 V, mass spectra are equivalent to operation with only MAB ionization. For time periods where the electron energy is 70 eV, the EI mechanism dominates the observed signal and the MAB ionization is treated as effectively negligible. Background peaks associated with EI of the discharge gas are removed by subtraction.

Source performance was optimized by two methods: aerosol mass spectral measurements and direct measurement of metastable species flux. MS experiments allow characterization of the instrument's analytical capabilities. The flux measurements allow the assembled source to be directly compared to other published designs (MS and non-MS applications).

For MS-based characterization oleic acid, $C_{18}H_{34}O_2$ (99.0% purity, Sigma Aldrich, St. Louis, MO) aerosols were created using a TSI constant output atomizer (St. Paul, MN, model 3076) and analyzed by the AMS using MAB ionization and EI. Aerosol concentrations were not calibrated. Instead, the sensitivity of MAB ionization relative to EI was used as a sensitivity metric.

For metastable species flux measurements, a Faraday cup detector [39,40] was mounted in the position of the AMS vaporizer–ionization chamber assembly with the metastable species beam directed at a stainless steel plate located at the back end of the detector cup. Collisions of metastable species with the surface cause the release of electrons. The generated replenishing current is measured with a picoammeter (model 6487, Keithley, Cleveland, OH) [41]. Electrodes in front of the stainless steel plate serve to deflect incoming electrons and ions, and to draw released electrons from the surface. A metastable species flux is calculated using the recorded electron current and geometry of the source and detector system, and assuming a metastable species-to-electron conversion factor of 0.13 ± 0.09 for Ar on stainless steel [42]. The Faraday cup detector was built with a 5 mm entrance aperture mimicking the through hole in the ion chamber, such that the measured current can be assumed approximately equal to the effective current of metastable species entering the ionization volume.

Field data are presented from the FLAME-3 experiment (Fire Lab at Missoula Experiment, Phase 3), which focused on quantification of emissions from controlled biomass burns simulating wildfires, and was conducted at the United States Forest Service's Fire Science Laboratory in Missoula, MT [43]. An HR-ToF-AMS equipped with the MAB source was positioned on the second story of the Fire Lab, and sampled directly (using a 20 m-long 3/8 inch OD copper inlet with a flow of 10 L min^{-1}) from a large smoke stack through which smoke was directed. Data are presented from an experiment where different materials were burned for ~5 min each.

3. Results and discussion

In the early stages of this work, features from multiple published metastable source designs [22,28,29,37,38,40,44–47] were explored to identify a design having high metastable flux, stability sufficient for field experiments (minimum of 12 h of continuous data acquisition), and repeatable performance. Factors that were varied included: cathode shape, electrode geometry, cathode material, and nozzle material. Those results are not detailed here, but interested readers are pointed to the referenced works, which discuss these designs. The presented results refer to the source described in Section 2.

3.1. Metastable source optimization

The gas jet exiting the discharge nozzle contains a mixture of neutral species, metastable species, ions, and electrons. Analyte molecules can be ionized by numerous mechanisms involving interactions with the charged species, most notably EI, which typically yields strong fragmentation. In order to simplify the ionization environment and allow Penning ionization to be the dominant mechanism, a combination of electric and magnetic fields is used to remove charged species from the beam directed into the AMS ionization volume. The first descriptions of MAB ionization and recent applications of beam source for metastable-induced fragmentation [32] used only electrostatic deflection. In this work, strong deflection fields alone proved insufficient. Fig. 2 shows a difference mass spectrum (particle beam transmitted data minus particle beam blocked data) of laboratory-generated oleic acid particles, collected using EI (Fig. 2a) and Ar^* MAB (M(Ar)B) ionization with and without the applied magnetic and electric deflection fields (Fig. 2b–e). When neither deflection plates nor a magnet are used (Fig. 2b) the MAB–AMS spectrum has a similar degree of fragmentation compared to the EI–AMS spectrum with the majority of the total signal below m/z 100, suggesting that ionization is dominated by discharge electrons. When only the deflection plate voltage is applied (Fig. 2c) the fraction of the signal from the parent plus dehydrated molecular ion (F_p) doubles, and there is an increase in the relative intensity of fragments above m/z 100. Simultaneously, deflection of charged species (Ar^+ and/or e^-) leads to a 23-fold reduction in total recorded ion current. Calculations suggest that the applied deflection voltages should be more than sufficient to deflect all of the Ar^+ and e^-, and operation at substantially higher voltages (up to 10×) results in little change in the spectrum. But, when a magnetic field is applied alone (Fig. 2d) or concurrent to the deflection plates (Fig. 2e), fragments below m/z 50 are nearly eliminated. It is clear that the magnets are more effectively removing electrons from the axis of the ionization volume, but the exact mechanism of removal is unknown. For instance, the magnets could be changing the nature of the discharge between the nozzle and skimmer, or the magnets could be removing electrons generated in processes downstream of the deflection plates (which could also explain the lack of efficiency of the deflection plates). Unless otherwise noted, both magnets and deflection plates were used for all data presented in the remainder of this paper. In future designs the deflection plates will not be incorporated into the design and only the magnets will be used.

The primary tunable parameters of the MAB ionization source are discharge current and discharge gas pressure. Metastable beam sources of similar design are typically run near 10 mA [22,37]. For our source, a current greater than 6 mA is required to maintain a stable discharge. Above a current of 16 mA oxidized material starts to form on the tip of the tungsten cathode, leading to rapid degradation and discharge failure. The metastable flux is approximately 30% greater at 16 mA than at 8 mA, and the observed MS ion current is directly proportional to this flux (Fig. S3). Typical experiments are run at 12 mA to ensure longer term stability.

Cathode chamber pressure varies greatly for Ar^* beam sources (40 [22] to 400 mbar [45]), depending on design geometry and pumping. For our source, a discharge cannot be maintained below 13 mbar and above 65 mbar the gas load becomes too high for the vacuum system. The effect of cathode chamber pressure in this range was characterized using an argon discharge for the ionization of oleic acid particles. Fig. 3 shows the total signal at m/z 40, 43, 264, and 282 as a function of cathode chamber pressure. These peaks correspond to Ar^+, an oleic acid fragment indicative

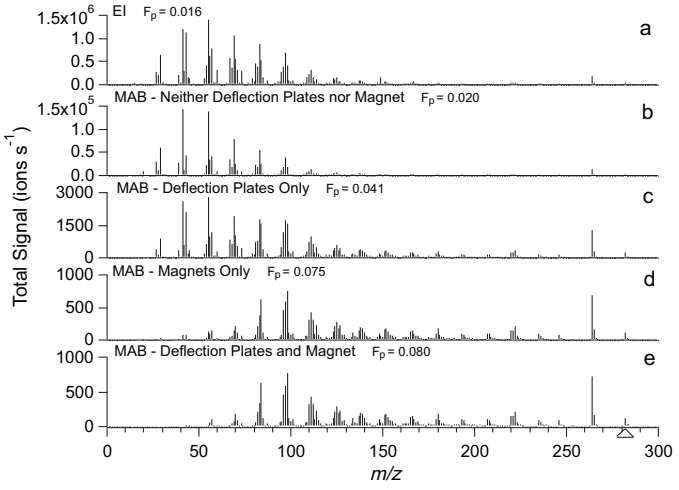

Fig. 2. Comparison of the background subtracted mass spectra of pure oleic acid aerosol standards acquired with a vaporizer temperature of 200 °C ionized by (a) EI (b) MAB without deflection or a magnet (c) MAB with only deflection plates, (d) MAB with only a magnet, and (e) MAB with a magnet and deflection plates in the experimental setup. F_p is the ratio of the signal from the parent plus dehydrated oleic acid ions to the total signal.

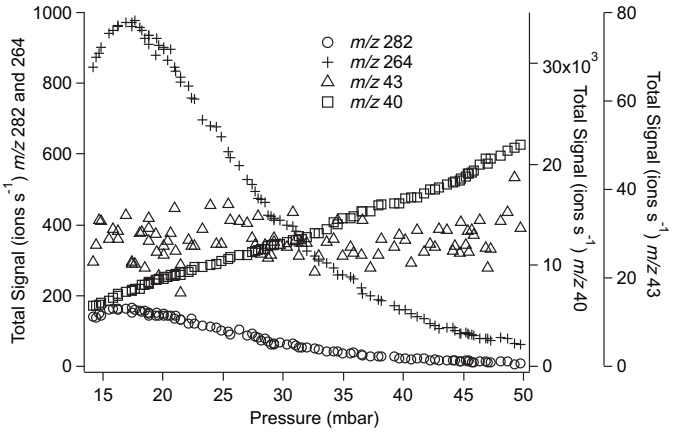

Fig. 3. Effect of the discharge gas pressure on AMS signals while using a constant concentration of pure oleic acid aerosol standards. m/z 40 corresponds to Ar^+. m/z 43 is a marker for highly fragmented oleic acid molecules. m/z 264 and 282 correspond to dehydrated oleic acid and the oleic acid parent ion, respectively.

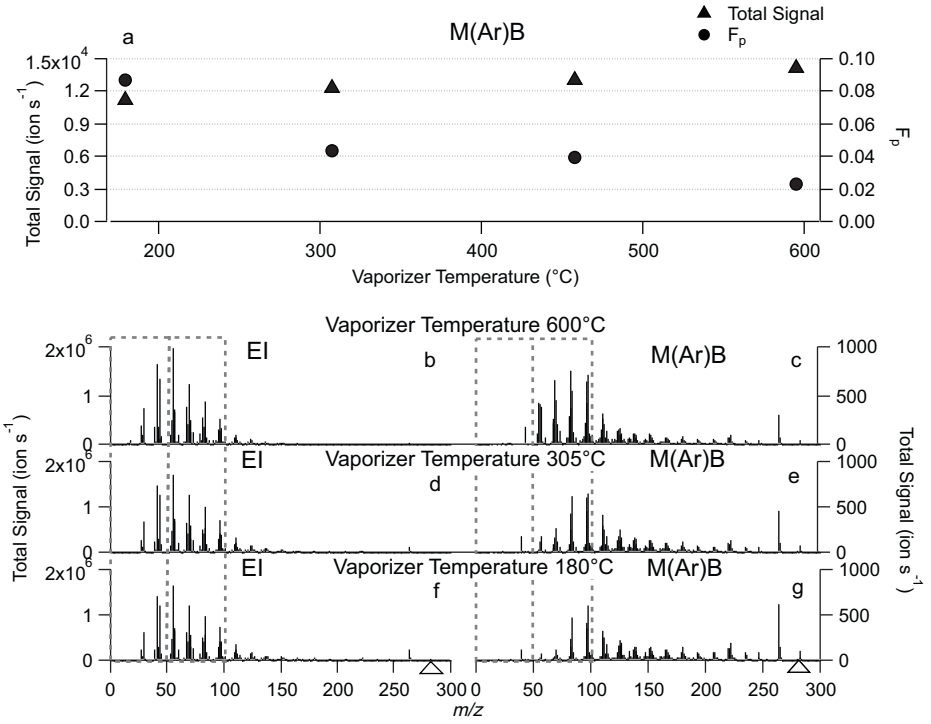

Fig. 4. Effect of AMS vaporizer temperature on the mass spectra of pure oleic acid aerosol standards: (a) normalized total ion signal and F_p vs. T_{vap}. (b–e) Pure oleic acid difference mass spectra obtained using (b) EI with T_{vap} = 600 °C; (c) M(Ar)B with T_{vap} = 600 °C; (d) EI with T_{vap} = 305 °C; (e) M(Ar)B with T_{vap} = 305 °C; (f) EI with T_{vap} = 180 °C; (g) M(Ar)B with T_{vap} = 180 °C.

of EI, dehydrated oleic acid, and the oleic acid parent ion, respectively. The EI indicator at m/z 43 displays no apparent pressure dependence. On the other hand, the parent and dehydrated parent peaks (m/z 282 and 264), which are presumed to originate by Penning ionization when electromagnetic deflection is enabled, both reach maximum intensity at ~17 mbar and then rapidly decrease in intensity. Metastable argon flux measurements show identical pressure dependence, reaching a maximum at 17 mbar and then decreasing with increased pressure, suggesting that this trend is due to the changes in metastable argon reaching the ionization volume. The observed reduction in metastable argon population is thought to be the result of collisional quenching [24].

3.2. Stability of the discharge

Atmospheric field studies, which have typical durations of 1 month [48,49], demand an ionization source that is stable and that yields reproducible performance day-to-day. Ar^* metastable flux was recorded for 3 weeks of continuous operation, with no adjustment to any source variables. The discharge demonstrated good stability with an average flux of 3.6×10^{13} sr^{-1} s^{-1} and 6% standard deviation, with a range of deviation of ±13% of the average value within this period (data shown in Fig. S4). Some fluctuations in flux correlated strongly with changes in cathode chamber pressure, which were possibly due to changes in laboratory temperature. During a separate experiment the ambient temperature at the AMS inlet was recorded and it was observed that changes in reagent gas pressure were correlated with temperature changes. Future work will implement automated pressure control to eliminate such fluctuations.

3.3. Fragmentation of organic compounds

The MAB ionization source was coupled to the AMS with the specific aim of reducing fragmentation in mass spectra of OA. For more standard gas-phase analysis conditions (e.g., GC) with a MAB ionization source, fragmentation of analyte ions is driven by excess internal energy acquired in the Penning ionization electron transfer reaction. In the MAB–AMS, metastable species are interacting with analyte molecules generated by a hot vaporizer in high vacuum. These molecules may acquire substantial internal energy during vaporization, leading to molecular decomposition before ionization and/or enhanced fragmentation after ionization. For the EI–AMS, the vaporizer temperature is typically set to 600 °C to ensure vaporization of all OA species and common inorganics. However, vaporizer temperatures as low as 180 °C are sufficient to evaporate about 75% of ambient OA species [50]. The effects of vaporization temperature on observed M(Ar)B-AMS oleic acid mass spectra are presented in Fig. 4. Fig. 4a shows the total ion signal recorded by the MAB–AMS as a function of temperature. For a fixed aerosol concentration, this reflects the efficiency of vaporization on the time scale of the measurement, and perhaps small differences in ionization efficiency of thermal decomposition products vs. the oleic acid molecule. Fig. 4a also shows F_p (the ratio of m/z 282 + m/z 264 to the total ion signal) as a function of vaporizer temperature. While the total ion current increases by 25%, F_p drops by a factor of 4 across the range between 180 and 600 °C, demonstrating the improved "softness" of analysis with reduced temperature vaporization. Fig. 4b–g displays mass spectra of oleic acid aerosols for 3 temperatures acquired using EI (70 eV) and M(Ar)B ionization. The fragmentation patterns of EI mass spectra are similar at the 3 temperatures, with the fraction of the signal above m/z 100 increasing only from 10% to 20% over the entire temperature range, most of the signal remaining below m/z 100, and F_p being at least five times smaller than for M(Ar)B at the same temperature. The M(Ar)B spectra are more sensitive to vaporizer temperature; at 600 °C 42% of the signal is above m/z 100, while at 180 °C 70% of the signal is above m/z 100 and at 305 °C the degree of fragmentation is in between those extremes. Even at 600 °C, the envelope of fragment ions is shifted to higher m/z than for EI (note for instance the difference in mass

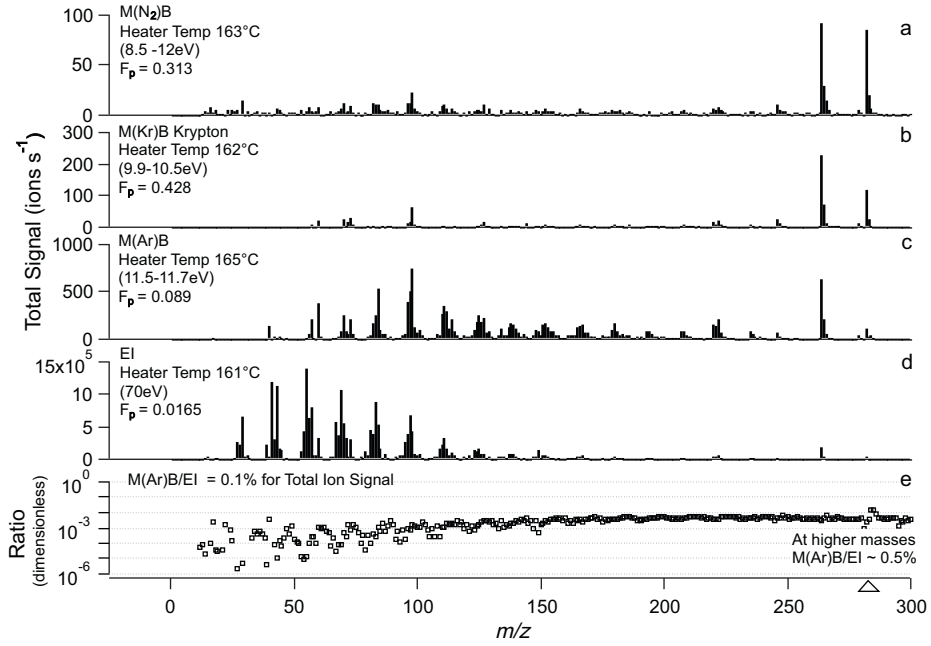

Fig. 5. Difference mass spectra of pure oleic acid aerosol standards using ionization by: (a) $M(N_2)B$; (b) M(Kr)B; (c) M(Ar)B; (d) EI. (e) Ratio of the signals of M(Ar)B/EI for each m/z.

spectra below m/z 50). Recognizing that optimum vaporization temperature and fragmentation vs. temperature will vary for the different components of heterogeneous OA sources, programmed vaporizer temperature ramping has been used in applications of the MAB–AMS.

The energy of the Penning ionization reaction can be adjusted by changing the discharge gas. This tunability can potentially be exploited to achieve selective ionization or to affect the degree of molecular fragmentation. The MAB–AMS has been used with beams of Ar^*, Kr^*, and N_2^*, which have primary excited state energies of 11.73 and 11.55 eV, 10.56 and 9.92 eV, and 8.45 and 6.22 eV [18], respectively. Fig. 5 compares the mass spectra of oleic acid aerosols measured with the MAB–AMS using these different discharge gases and EI with a vaporizer temperature of $165 \pm 5\,^{\circ}C$ (which is the lowest temperature that can be achieved with the ionizer operating at normal emission current and no heating current applied to the vaporizer). F_p values are reported for each mass spectrum. As expected, observed fragmentation decreases with metastable species excited state energy. The dominant state(s) of N_2^* produced in this discharge are unknown, but the qualitative appearance of the spectra suggest that the effective energies are similar to that of Kr^*. The total recorded ion signal is approximately equal for Kr^* and N_2^*, and is about 5% of that observed with Ar*. Sensitivity relative to EI is discussed below.

Northway et al. [16] published F_p values for oleic acid analysis with the VUV–AMS at several photon energies and vaporizer temperatures, using tunable synchrotron radiation. For 10.0 eV, which is a primary emission energy of the Kr lamp, F_p was 0.45 at 200 °C and 0.55 at 140 °C. This can be compared to the 0.31, 0.42, and 0.09 for N_2, Kr, and Ar discharges, respectively, each near 165 °C. Qualitatively, the VUV spectra obtained with the lamp, having dominant lines at 10.0 and 10.6 eV, appear very similar to the M(Kr)B-AMS data.

3.4. Sensitivity of MAB–AMS

Fig. 5e compares the recorded signal intensities for M(Ar)B and EI at each m/z in the oleic acid mass spectra. At m/z values greater than 150, M(Ar)B signals are approximately 0.5% of EI, while the total ion current over all m/z values is 0.1% of EI. This relative signal intensity is far below the 20% reported by Faubert [22]. This discrepancy could be due to either differences in operating conditions of the EI sources, or in the intensities of the metastable beams reaching the ionization volumes. The operating conditions of the EI source were not described in that work, but a He^* flux of $(1.2–1.5) \times 10^{15}\ sr^{-1}\ s^{-1}$ was reported. Literature values for other Ar^* beam sources range between 10^{12} and $10^{15}\ sr^{-1}\ s^{-1}$ [28,38,45]. These values can be compared to the flux of the MAB–AMS source, which is typically $3.6^{+8.1}_{-1.5} \times 10^{13}\ \ sr^{-1}\ \ s^{-1}$. The 30 times lower flux (uncertainty range 10–50) at the ionization volume of the MAB–AMS source compared with the best Ar^* literature source could reasonably explain most of the 2 orders of magnitude difference in relative MAB/EI sensitivities, with the rest of the difference potentially due to differences in the EI sources in the two studies. The cause of the lower flux is unclear, but may be related to the differences in source geometry or pumping conditions between this source and the best performing sources. These parameters will be explored in future optimization of the MAB source.

The M(Ar)B/EI ratio of 0.1% represents an improvement over the reported 0.02% which was reported for the VUV–AMS system [16]. And, importantly, it is expected that this sensitivity can be increased with improvements in the metastable beam source design. The detection limit for organic aerosols (OA) of the EI–AMS used in this work is approximately 0.1 $\mu g\,m^{-3}$ (5 min averages). For a MAB/EI signal ratio of 0.1%, the detection limit of the MAB–AMS can be estimated (proportionally to the square root of the signal) as 3.1 $\mu g\,m^{-3}$, which is sufficient for sampling aerosol sources, such as biomass burning smoke, vehicle emissions, and smog chamber aerosol, at typical concentrations of a few hundred $\mu g\,m^{-3}$ [43]. However the current MAB–AMS sensitivity would not provide practical time resolution for sampling in rural, remote, or even polluted urban conditions (where ambient OA concentrations are in the range of 5–20 $\mu g\,m^{-3}$ [51]).

3.5. FLAME-3 field campaign

As a first field deployment, the MAB–AMS was run during the 1-month FLAME-3 campaign, which measured emissions of con-

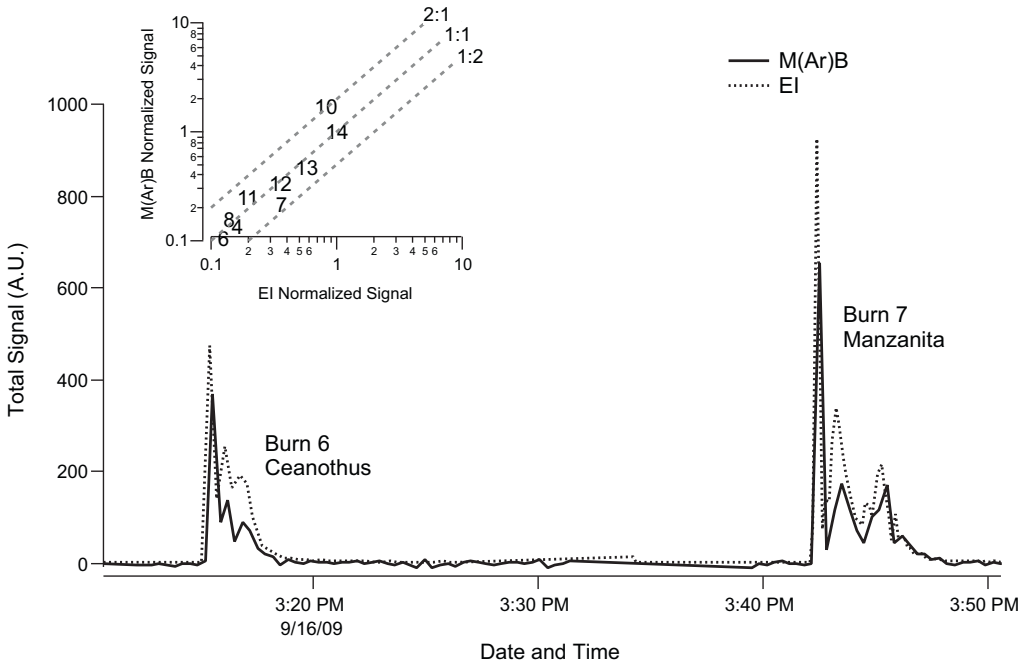

Fig. 6. Comparison of the time series of total M(Ar)B and EI instrument OA signals for two burns. Inset: scatter plot of the integrated signals from M(Ar)B and EI for nine biomass burns. Data have been normalized to the total ion signal of burn 14. Note that due to the use of two separate inlets, perfect correspondence of the concentration time series is not expected.

trolled biomass burns. Fig. 6 compares M(Ar)B-AMS signal to data from a separate EI–AMS, operated by Colorado State University, that was sampling in parallel through a second inlet located at a different location on the exhaust stack [52]. The time series shows total mass spectral signal across two burns. Features in the two traces are similar, suggesting that Ar^* are ionizing the major species in the burn emissions. The inset compares the total organic aerosol signal recorded by each instrument for a larger collection of burns. Burns are indicated by number, and each number is a different fuel. The ratio of the signals from the two instruments is constant within a factor of 3. Given that slightly different smoke concentrations were sampled due to the different inlet locations, this suggests that MAB–AMS has near linear response to changes in OA concentration for the very diverse types of OA produced when burning different biomasses [43,52]. Mass spectra for lodgepole pine smoke (a complex mixture of organic molecules) analyzed with EI, M(Ar)B, M(Kr)B, and M(N_2)B ionization are shown in Figs. S5 and S6. MAB spectra of smoke have enhanced signal at higher m/z in comparison to the EI spectrum. In addition, molecular and marker ions become more distinctly resolved in MAB, even though they may be present at higher intensity for EI, due to the reduced contribution of fragment ions at neighboring m/z.

4. Conclusions

A MAB ionization source has been coupled to an Aerodyne time-of-flight aerosol mass spectrometer. The source design allows real-time alternation between MAB and electron ionization. The discharge was demonstrated to be stable for several weeks, which is a requirement for extended field studies. Ionization with a discharge of Ar, Kr or N_2 generates less molecular fragmentation than similar analysis with EI, which could enable the detection of different components via factor analysis and thus potentially increase information about OA. M(Kr)B is the softest, while M(Ar)B ionization is the most sensitive of the three gases, producing total ion signal that is 0.1% of that achieved with EI. This relative sensitivity is lower than that reported for previous implementations of MAB ionization, but is consistent with the metastable flux recorded for the MAB–AMS discharge. The sensitivity of the current system is sufficient for concentrated laboratory conditions, but impractical for ambient sampling. Future work will focus on improving the intensity of the discharge and the transmission of the metastable beam into the ionization volume of the mass spectrometer, so that application to ambient OA becomes practical. Based on published characterization of other metastable beam sources, it is believed that up to a factor of 30 improvement in signal intensity could be achieved.

Acknowledgements

This research was funded by a Seed Grant from the University of Colorado-Boulder, NOAA OGP grant NA08OAR4310565, CARB CalNex funding, EPA STAR grant R833747, and NSF grants ATM-0449815 and ATM-0919189. CBR is grateful for NASA ESSF Graduate Fellowship (NNX09AO29H). We thank James Whitby (Tofwerk) and Claude Beaugrand (Abionix) for useful discussions, members of the Jimenez Group for technical support, Taehyoung Lee, Jeff L. Collett, and Sonia M. Kreidenweis from Colorado State University for the use of their data for MAB-EI comparisons, and Kip Carrico of CSU, and Emily Lincoln, Cycle Wold, and Wei-Min Hao of the Fire Lab staff for the organization of the FLAME-3 campaign.

Appendix A. Supplementary data

Supplementary data associated with this article can be found, in the online version, at doi:10.1016/j.ijms.2011.01.027.

References

[1] P. Forster, V. Ramaswamy, P. Artaxo, T. Berntsen, R. Betts, D.W. Fahey, J. Haywood, J. Lean, D.C. Lowe, G. Myhre, J. Nganga, R. Prinn, G. Raga, M. Schulz and R. Van Dorland, 2007. Changes in Atmospheric Constituents and in Radiative Forcing. in: S. Solomon, D. Qin, M. Manning, Z. Chen, M. Marquis, K.B. Averyt, M.Tignor and H.L. Miller (Eds.), Climate Change 2007: The Physical Science Basis. Contribution of Working Group I to the Fourth Assessment Report of

the Intergovernmental Panel on Climate Change. Cambridge University Press, Cambridge, United Kingdom and New York, NY, USA, 2007, pp. 129–234.
[2] M. Hallquist, J.C. Wenger, U. Baltensperger, Y. Rudich, D. Simpson, M. Claeys, J. Dommen, N.M. Donahue, C. George, A.H. Goldstein, J.F. Hamilton, H. Herrmann, T. Hoffmann, Y. Iinuma, M. Jang, M.E. Jenkin, J.L. Jimenez, A. Kiendler-Scharr, W. Maenhaut, G. McFiggans, T.F. Mentel, A. Monod, A.S.H. Prevot, J.H. Seinfeld, J.D. Surratt, R. Szmigielski, J. Wildt, The Formation, properties and impact of secondary organic aerosol: current and emerging issues, Atmospheric Chemistry and Physics 9 (2009) 5155–5236.
[3] J.C. Chow, J.G. Watson, L.C. Pritchett, W.R. Pierson, C.A. Frazier, R.G. Purcell, The DRI thermal optical reflectance carbon analysis system – description, evaluation and applications in United-States air-quality studies, Atmospheric Environment 27 (1993) 1185–1201.
[4] A.P. Sullivan, R.J. Weber, A.L. Clements, J.R. Turner, M.S. Bae, J.J. Schauer, A method for on-line measurement of water-soluble organic carbon in ambient aerosol particles: results from an urban site, Geophysical Research Letters 31 (2004).
[5] B.J. Williams, A.H. Goldstein, D.B. Millet, R. Holzinger, N.M. Kreisberg, S.V. Hering, A.B. White, D.R. Worsnop, J.D. Allan, J.L. Jimenez, Chemical speciation of organic aerosol during the international consortium for atmospheric research on transport and transformation 2004: results from in situ measurements, Journal of Geophysical Research: Atmospheres 112 (2007).
[6] S. Gilardoni, S. Liu, S. Takahama, L.M. Russell, J.D. Allan, R. Steinbrecher, J.L. Jimenez, P.F. De Carlo, E.J. Dunlea, D. Baumgardner, Characterization of organic ambient aerosol during MIRAGE 2006 on three platforms, Atmospheric Chemistry and Physics 9 (2009) 5417–5432.
[7] S. Decesari, M. Mircea, F. Cavalli, S. Fuzzi, F. Moretti, E. Tagliavini, M.C. Facchini, Source attribution of water-soluble organic aerosol by nuclear magnetic resonance spectroscopy, Environmental Science & Technology 41 (2007) 2479–2484.
[8] M.R. Canagaratna, J.T. Jayne, J.L. Jimenez, J.D. Allan, M.R. Alfarra, Q. Zhang, T.B. Onasch, F. Drewnick, H. Coe, A. Middlebrook, A. Delia, L.R. Williams, A.M. Trimborn, M.J. Northway, P.F. DeCarlo, C.E. Kolb, P. Davidovits, D.R. Worsnop, Chemical and microphysical characterization of ambient aerosols with the aerodyne aerosol mass spectrometer, Mass Spectrometry Reviews 26 (2007) 185–222.
[9] B. Oktem, M.P. Tolocka, M.V. Johnston, On-line analysis of organic components in fine and ultrafine particles by photoionization aerosol mass spectrometry, Analytical Chemistry 76 (2004) 253–261.
[10] R. Holzinger, J. Williams, F. Herrmann, J. Lelieveld, N.M. Donahue, T. Rockmann, Aerosol analysis using a thermal-desorption proton-transfer-reaction mass spectrometer (TD–PTR–MS): a new approach to study processing of organic aerosols, Atmospheric Chemistry and Physics 10 (2010) 2257–2267.
[11] T. Thornberry, D.M. Murphy, D.S. Thomson, J. de Gouw, C. Warneke, T.S. Bates, P.K. Quinn, D. Coffman, Measurement of aerosol organic compounds using a novel collection/thermal-desorption PTR-ITMS instrument, Aerosol Science and Technology 43 (2009) 486–501.
[12] R.L.N. Yatavelli, J.A. Thornton, Particulate organic matter detection using a micro-orifice volatilization impactor coupled to a chemical ionization mass spectrometer (MOVI-CIMS), Aerosol Science and Technology 44 (2010) 61–74.
[13] J.D. Hearn, G.D. Smith, Kinetics and product studies for ozonolysis reactions of organic particles using aerosol CIMS, Journal of Physical Chemistry A 108 (2004) 10019–10029.
[14] B.W. LaFranchi, J. Zahardis, G.A. Petrucci, Photoelectron resonance capture ionization mass spectrometry: a soft ionization source for mass spectrometry of particle-phase organic compounds, Rapid Communications in Mass Spectrometry 18 (2004) 2517–2521.
[15] I.M. Ulbrich, M.R. Canagaratna, Q. Zhang, D.R. Worsnop, J.L. Jimenez, Interpretation of organic components from positive matrix factorization of aerosol mass spectrometric data, Atmospheric Chemistry and Physics 9 (2009) 2891–2918.
[16] M.J. Northway, J.T. Jayne, D.W. Toohey, M.R. Canagaratna, A. Trimborn, K.I. Akiyama, A. Shimono, J.L. Jimenez, P.F. DeCarlo, K.R. Wilson, D.R. Worsnop, Demonstration of a VUV lamp photoionization source for improved organic speciation in an aerosol mass spectrometer, Aerosol Science and Technology 41 (2007) 828–839.
[17] F.M. Penning, Ionisation by metastable atoms, Naturwissenschaften 15 (1927) 818.
[18] D.W. Setser, Reactive Intermediates in the Gas Phase, Acadenic Press, Inc., New York City, 1979.
[19] D.R. Anderson, V.M. Bierbaum, C.H. Depuy, J.J. Grabowski, Flowing afterglow studies of organic positive-ions generated by penning ionization using metastable argon atoms, International Journal of Mass Spectrometry and Ion Processes 52 (1983) 65–94.
[20] A. Lofthus, P.H. Krupenie, Spectrum of molecular nitrogen, Journal of Physical and Chemical Reference Data 6 (1977) 113–307.
[21] M.G. Ikonomou, S. Rayne, Chromatographic and ionization properties of polybrominated diphenyl ethers using GC/high-resolution Ms with metastable atom bombardment and electron impact ionization, Analytical Chemistry 74 (2002) 5263–5272.
[22] D. Faubert, G.J.C. Paul, J. Giroux, M.J. Bertrand, Selective fragmentation and ionization of organic-compounds using an energy-tunable rare-gas metastable beam source, International Journal of Mass Spectrometry and Ion Processes 124 (1993) 69–77.
[23] T.M. Reed, The ionization potential and the polarizability of molecules, Journal of Physical Chemistry 59 (1955) 428–432.
[24] K. Hiraoka, H. Furuya, S. Kambara, S. Suzuki, Y. Hashimoto, A. Takamizawa, Atmospheric-pressure Penning ionization of aliphatic hydrocarbons, Rapid Communications in Mass Spectrometry 20 (2006) 3213–3222.
[25] Z.J. Wu, J.X. Pu, L.M. Li, D.M. Fang, H.Y. Qi, J.Z. Chen, G.Y. Li, H.D. Sun, G.L. Zhang, Electrospray tandem mass spectrometry of longipedlactone triterpenoids, Journal of Mass Spectrometry 45 (2010) 451–455.
[26] F.J. Andrade, J.T. Shelley, W.C. Wetzel, M.R. Webb, G. Gamez, S.J. Ray, G.M. Hieftje, Atmospheric pressure chemical ionization source. 1. Ionization of compounds in the gas phase, Analytical Chemistry 80 (2008) 2646–2653.
[27] R.B. Cody, J.A. Laramee, H.D. Durst, Versatile new ion source for the analysis of materials in open air under ambient conditions, Analytical Chemistry 77 (2005) 2297–2302.
[28] D.W. Fahey, W.F. Parks, L.D. Schearer, High-flux beam source of thermal rare-gas metastable atoms, Journal of Physics E-Scientific Instruments 13 (1980) 381–383.
[29] J.Q. Searcy, Supersonic molecular-beam metastable atom source initiated by direct discharge, Review of Scientific Instruments 45 (1974) 589–590.
[30] M.J. Bertrand, D. Faubert, O. Peraldi, A. L'Heureux, U.S. Patent 6,124,675, 2000.
[31] C. Le Vot, C. Afonso, C. Beaugrand, J.C. Tabet, Implementation of a Penning ionization source on a FTICR instrument with ion funnel optics, International Journal of Mass Spectrometry, in press.
[32] V.D. Berkout, Fragmentation of protonated peptide ions via interaction with metastable atoms, Analytical Chemistry 78 (2006) 3055–3061.
[33] P. Liu, P.J. Ziemann, D.B. Kittelson, P.H. McMurry, Generating particle beams of controlled dimensions and divergence. 1. Theory of particle motion in aerodynamic lenses and nozzle expansions, Aerosol Science and Technology 22 (1995) 293–313.
[34] J.T. Jayne, D.C. Leard, X.F. Zhang, P. Davidovits, K.A. Smith, C.E. Kolb, D.R. Worsnop, Development of an aerosol mass spectrometer for size and composition analysis of submicron particles, Aerosol Science and Technology 33 (2000) 49–70.
[35] F. Drewnick, S.S. Hings, P. DeCarlo, J.T. Jayne, M. Gonin, K. Fuhrer, S. Weimer, J.L. Jimenez, K.L. Demerjian, S. Borrmann, D.R. Worsnop, A new time-of-flight aerosol mass spectrometer (ToF-AMS) – instrument description and first field deployment, Aerosol Science and Technology 39 (2005) 637–658.
[36] P.F. DeCarlo, J.R. Kimmel, A. Trimborn, M.J. Northway, J.T. Jayne, A.C. Aiken, M. Gonin, K. Fuhrer, T. Horvath, K.S. Docherty, D.R. Worsnop, J.L. Jimenez, Field-deployable, high-resolution, time-of-flight aerosol mass spectrometer, Analytical Chemistry 78 (2006) 8281–8289.
[37] M. Baker, A.J. Palmer, R.T. Sang, A high flux metastable atomic discharge source with three-dimensional translation, Measurement Science & Technology 14 (2003) N5–N8.
[38] A.J. Palmer, M. Baker, R.T. Sang, Quantitative comparison of rare-gas cold cathode discharge metastable atomic beam sources, Review of Scientific Instruments 75 (2004) 5056–5058.
[39] N. Traitler, Design and Characterisation of a Metastable Helium Source, Physics Department, University of York, York, UK, 2002.
[40] J.P. Ashmore, R.T. Sang, Cathode design for a low-velocity metastable neon cold cathode discharge source, Measurement Science & Technology 12 (2001) N17–N21.
[41] F.B. Dunning, R.D. Rundel, R.F. Stebbings, Determination of secondary-electron ejection coefficients for rare-gas metastable atoms, Review of Scientific Instruments 46 (1975) 697–701.
[42] S. Schohl, D. Klar, T. Kraft, H.A.J. Meijer, M.W. Ruf, U. Schmitz, S.J. Smith, H. Hotop, Absolute detection of metastable rare-gas atoms by a CW laser photoionization method, Zeitschrift Fur Physik D-Atoms Molecules and Clusters 21 (1991) 25–39.
[43] G.R. McMeeking, S.M. Kreidenweis, S. Baker, C.M. Carrico, J.C. Chow, J.L. Collett, W.M. Hao, A.S. Holden, T.W. Kirchstetter, W.C. Malm, H. Moosmuller, A.P. Sullivan, C.E. Wold, Emissions of trace gases and aerosols during the open combustion of biomass in the laboratory, Journal of Geophysical Research: Atmospheres 114 (2009).
[44] J. Kawanaka, M. Hagiuda, K. Shimizu, F. Shimizu, H. Takuma, Generation of an intense low-velocity metastable-neon atomic-beam, Applied Physics B 56 (1993) 21–24.
[45] E.L. Leasure, C.R. Mueller, T.Y. Ridley, Hot, metastable atom, molecular-beam source, Review of Scientific Instruments 46 (1975) 635–637.
[46] F.P. Dos Santos, F. Perales, J. Leonard, A. Sinatra, J. Wang, F.S. Pavone, E. Rasel, C.S. Unnikrishnan, M. Leduc, Efficient magneto-optical trapping of a metastable helium gas, European Physical Journal: Applied Physics 14 (2001) 69–76.
[47] M. DeKieviet, M. Durr, S. Epp, F. Lang, M. Theis, Source for atomic beams of metastable gases: design and performance, Review of Scientific Instruments 75 (2004) 345–348.
[48] J.L. Jimenez, M.R. Canagaratna, N.M. Donahue, A.S.H. Prevot, Q. Zhang, J.H. Kroll, P.F. DeCarlo, J.D. Allan, H. Coe, N.L. Ng, A.C. Aiken, K.S. Docherty, I.M. Ulbrich, A.P. Grieshop, A.L. Robinson, J. Duplissy, J.D. Smith, K.R. Wilson, V.A. Lanz, C. Hueglin, Y.L. Sun, J. Tian, A. Laaksonen, T. Raatikainen, J. Rautiainen, P. Vaattovaara, M. Ehn, M. Kulmala, J.M. Tomlinson, D.R. Collins, M.J. Cubison, E.J. Dunlea, J.A. Huffman, T.B. Onasch, M.R. Alfarra, P.I. Williams, K. Bower, Y. Kondo, J. Schneider, F. Drewnick, S. Borrmann, S. Weimer, K. Demerjian, D. Salcedo, L. Cottrell, R. Griffin, A. Takami, T. Miyoshi, S. Hatakeyama, A. Shimono, J.Y. Sun, Y.M. Zhang, K. Dzepina, J.R. Kimmel, D. Sueper, J.T. Jayne, S.C. Herndon, A.M. Trimborn, L.R. Williams, E.C. Wood, A.M. Middlebrook, C.E. Kolb, U. Baltensperger, D.R. Worsnop, Evolution of organic aerosols in the atmosphere, Science 326 (2009) 1525–1529.

[49] Q. Zhang, J.L. Jimenez, M.R. Canagaratna, J.D. Allan, H. Coe, I. Ulbrich, M.R. Alfarra, A. Takami, A.M. Middlebrook, Y.L. Sun, K. Dzepina, E. Dunlea, K. Docherty, P.F. DeCarlo, D. Salcedo, T. Onasch, J.T. Jayne, T. Miyoshi, A. Shimono, S. Hatakeyama, N. Takegawa, Y. Kondo, J. Schneider, F. Drewnick, S. Borrmann, S. Weimer, K. Demerjian, P. Williams, K. Bower, R. Bahreini, L. Cottrell, R.J. Griffin, J. Rautiainen, J.Y. Sun, Y.M. Zhang, D.R. Worsnop, Ubiquity and dominance of oxygenated species in organic aerosols in anthropogenically-influenced northern hemisphere midlatitudes, Geophysical Research Letters 34 (2007).

[50] J.A. Huffman, K.S. Docherty, A.C. Aiken, M.J. Cubison, I.M. Ulbrich, P.F. DeCarlo, D. Sueper, J.T. Jayne, D.R. Worsnop, P.J. Ziemann, J.L. Jimenez, Chemically-resolved aerosol volatility measurements from two megacity field studies, Atmospheric Chemistry and Physics 9 (2009) 7161–7182.

[51] A.C. Aiken, D. Salcedo, M.J. Cubison, J.A. Huffman, P.F. DeCarlo, I.M. Ulbrich, K.S. Docherty, D. Sueper, J.R. Kimmel, D.R. Worsnop, A. Trimborn, M. Northway, E.A. Stone, J.J. Schauer, R.M. Volkamer, E. Fortner, B. de Foy, J. Wang, A. Laskin, V. Shutthanandan, J. Zheng, R. Zhang, J. Gaffney, N.A. Marley, G. Paredes-Miranda, W.P. Arnott, L.T. Molina, G. Sosa, J.L. Jimenez, Mexico city aerosol analysis during MILAGRO using high resolution aerosol mass spectrometry at the urban supersite (T0). Part 1. Fine particle composition and organic source apportionment, Atmospheric Chemistry and Physics 9 (2009) 6633–6653.

[52] T. Lee, A.P. Sullivan, L. Mack, J.L. Jimenez, S.M. Kreidenweis, T.B. Onasch, D.R. Worsnop, W. Malm, C.E. Wold, W.M. Hao, J.L. Collett, Variation of Chemical Smoke Marker Emissions During Flaming vs. Smoldering Phases of Laboratory Open Burning of Wildland Fuels, Aerosol Science and Technology 44 (2010) i–v.

Supplemental Information for the Manuscript:

Thermal Desorption Metastable Atom Bombardment Ionization Aerosol Mass Spectrometer

Carly B. Robinson[a,b], Joel R. Kimmel[b,c,d,*], Donald E. David[a,b], John T. Jayne[c], Achim Trimborn[c], Douglas R. Worsnop[c], and Jose L. Jimenez[a,b]

[a] Department of Chemistry and Biochemistry, University of Colorado, Boulder, CO

[b] Cooperative Institute for Research in Environmental Sciences (CIRES), University of Colorado, Boulder, CO

[c] Aerodyne Research Inc., Billerica, MA

[d] Tofwerk AG, Thun, Switzerland

Figure S1. Schematic of the HR-ToF-AMS and of the coupling of the MAB source.

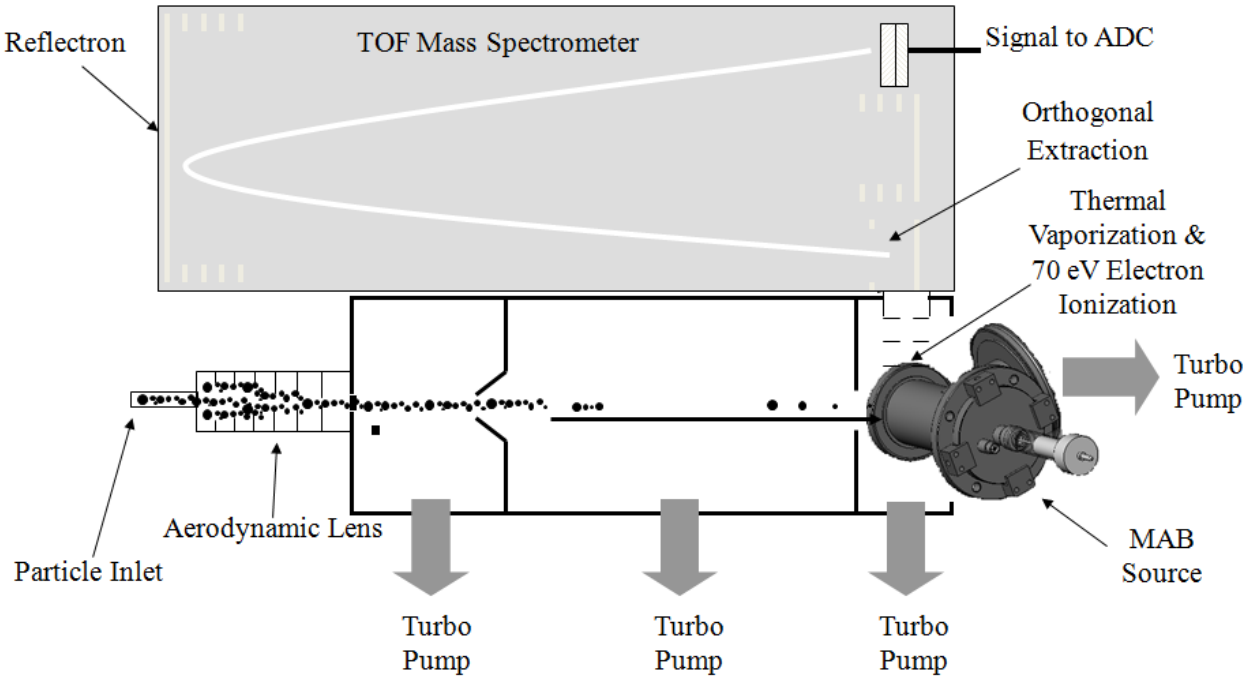

Figure S2. Metastable beam source design.

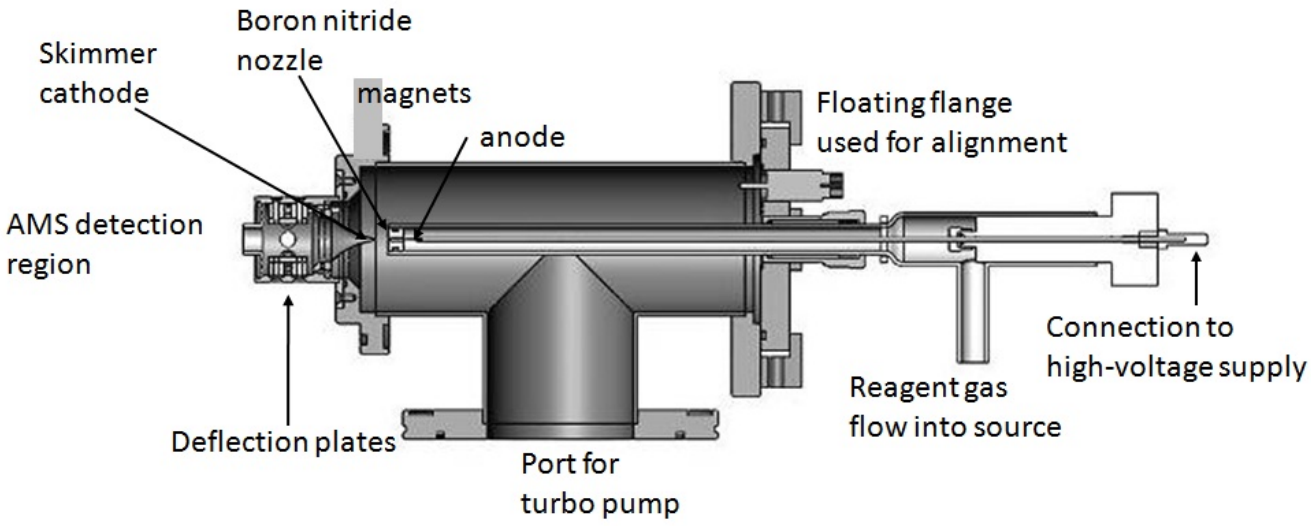

Figure S3. Effect of the discharge current on observed metastable species flux and on total MS signal when sampling a constant concentration of pure oleic acid aerosol standards. The left, black axis is the observed Ar^* induced current at the Faraday detector. The right, gray axis is the total MS signal.

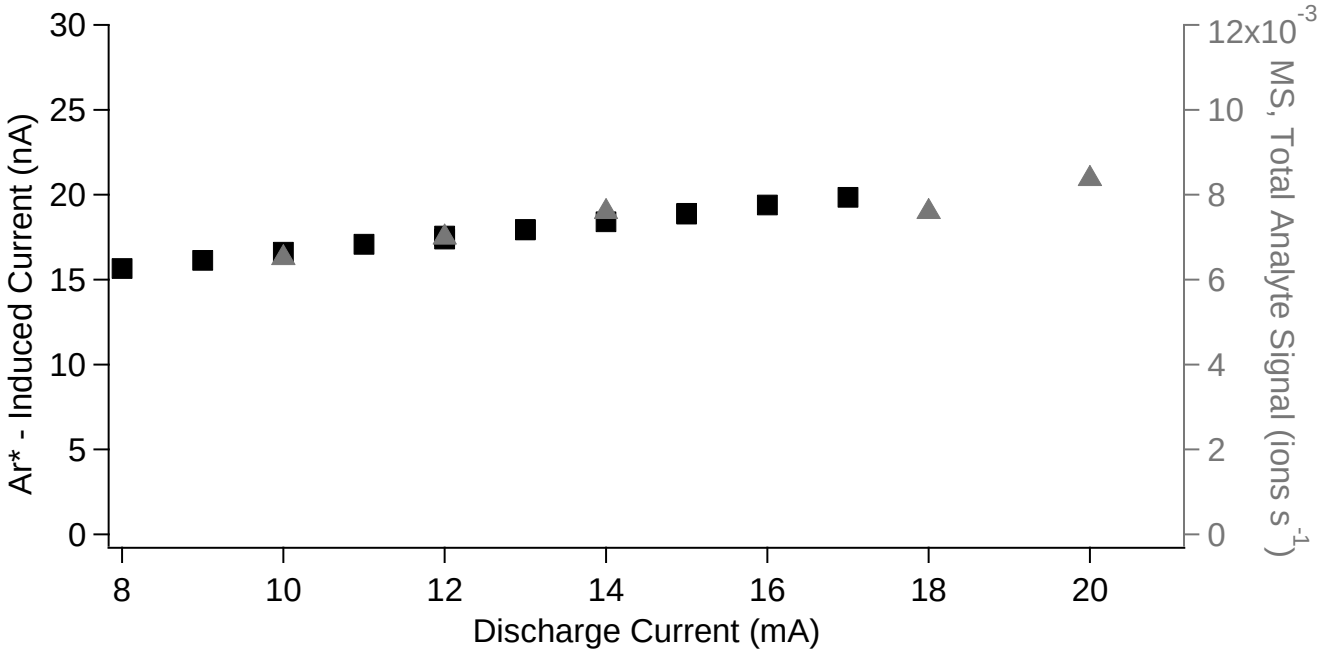

Figure S4. Metastable argon flux (gray, left-axis) and argon cathode chamber pressure (black, right-axis) over a period of 3 weeks of continuous operation.

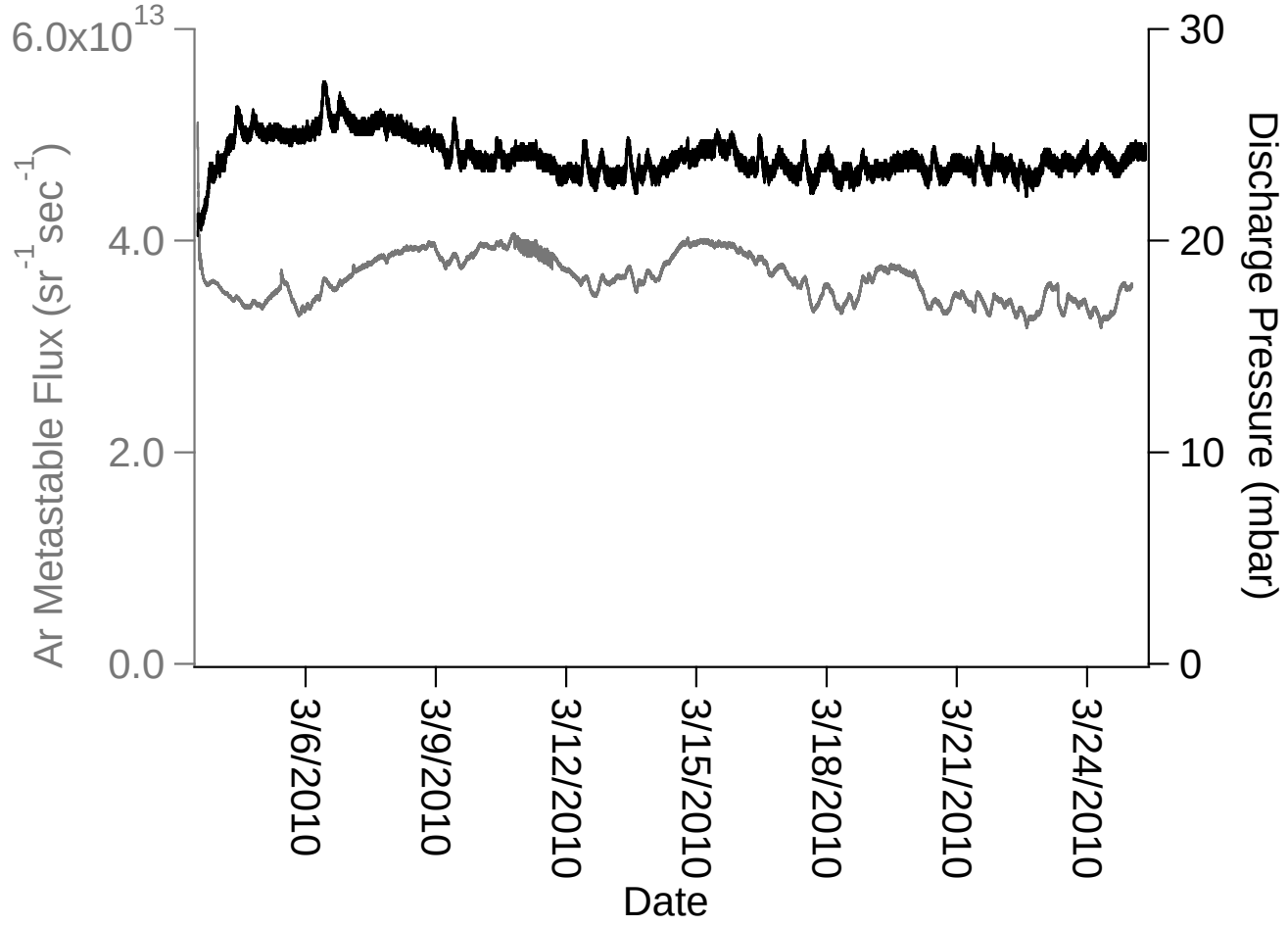

Figure S5. Background-subtracted mass spectra of Lodgepole Pine smoke using ionization by: (a)EI; (b) M(Ar)B; (c) M(Kr)B; (d) M(N_2)B. Marker ions consistent with those generated by the biomass burning molecular tracers levoglucosan (*m/z* 98 and 144) and abietic acid (*m/z* 302) are highlighted. MAB spectra of smoke have enhanced signal at higher *m/*z in comparison to the EI spectrum.

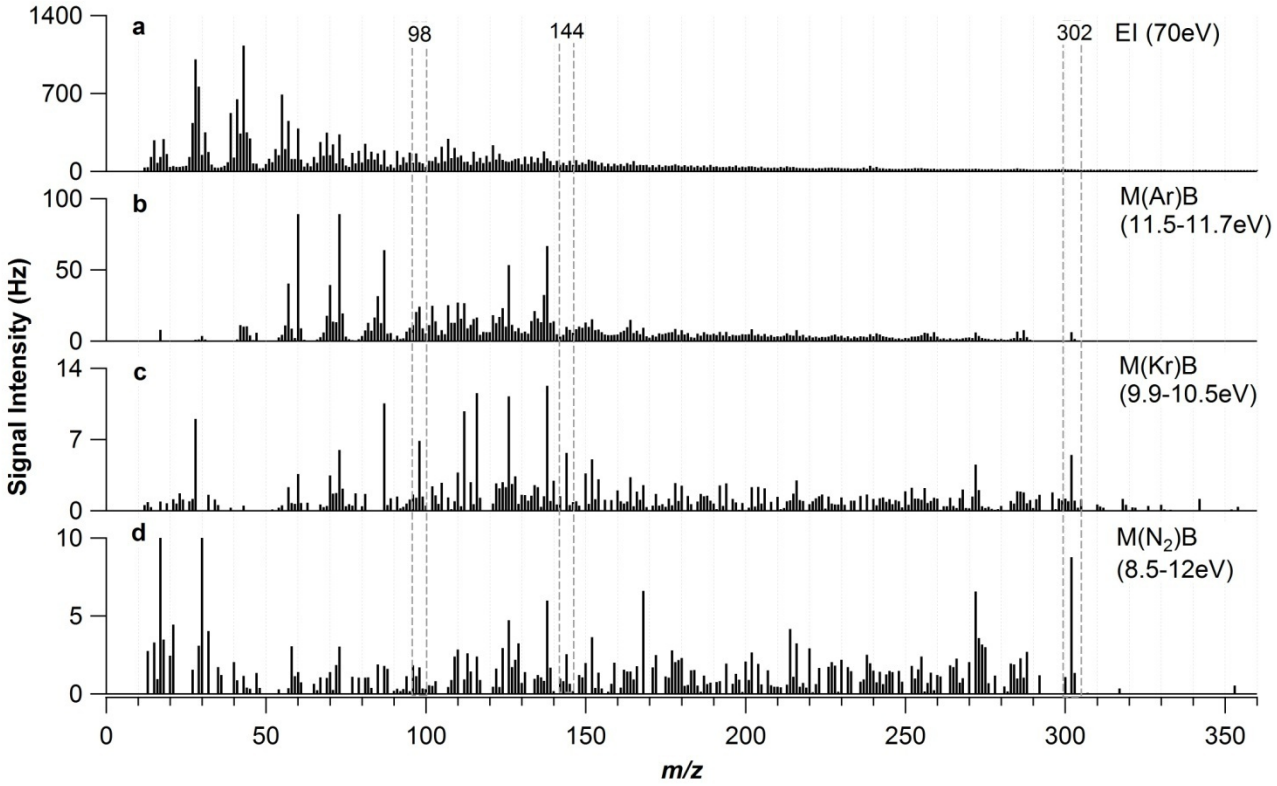

Figure S6. Same mass spectra shown in Figure S5, expanding in the range *m/z* 50 to 300, to emphasize high *m/z* ions. Marker ions consistent with those generated by the biomass burning molecular tracers levoglucosan (*m/z* 98 and 144) and abietic acid (*m/z* 302) are highlighted. These peaks become more distinctly resolved in MAB, even though they may be present at higher intensity for EI, due to the reduced contribution of fragment ions at neighboring *m/z*.